This article has been accepted for publication in a future issue of this journal, but has not been fully edited. Content may change prior to final publication. Citation information: DOI 10.1109/JSEN.2018.2879099, IEEE Sensors Journal

A Self-calibration Method for Angular Displacement Sensor Working in Harsh Environments

Li Gou, Donglin Peng, Xihou Chen, Liang Wu, and Qifu Tang

***Abstract*—This paper presents a new self-calibration method for angular displacement sensor, named coaxial sensors relative rotation (CSRR) method, which is suitable for sensors working in harsh environments. With a few slight modifications to the machine, CSRR method can also self-calibrate sensors on their application axes. This method works with two sensors. One sensor provides a benchmark and the other provides relative rotation against the benchmark, then each sensor can be self-calibrated by measuring the synchronized angular displacements of sensors and calculating the relative rotation angles. Experimental results indicate that this method is insensitive to relative rotation error of the two coaxial sensors, and it is also insensitive to sampling uniformity in particular situation. In that particular situation, the calibration accuracy can be better than ±2″ when the system error of sensor is about ±650″. Compared with equal division averaged (EDA) method, CSRR method mostly requires fewer sensors to get the same calibration accuracy; and compared with time-measurement dynamic reversal (TDR) method, CSRR method performs better on the axis supported by rolling bearing. What is more, we propose an evaluation indicator $|Y_{\Omega}|$ to evaluate the effective range of the CSRR method, and the $|Y_{\Omega}|$ makes it easier for others to determine whether this method is suitable for their applications.**

***Index Terms*—self-calibration, angular displacement sensor, relative rotation, sampling uniformity, effective range.**

I. Introduction

In an industrial rotary system, the calibration is required to maintain high precision state for angular displacement sensors [1], [2]. However, most calibrations rely on expensive angle comparators, which require high maintenance costs [3]-[6]; and they are usually performed on calibration axes with elaborate devices, not on the application axes, which lead to additional errors caused by the sensor transmissions from calibration devices to machines [7]-[9]. Thus, a simple self-calibration method, which keeps the angular displacement sensors always on its application axis and allows them to maintain high precision without angle comparators, can be one of means to solve the above-mentioned problems [10]- [12].

To make self-calibration method credible, two methods, EDA and Ernst [13], [14], have been realized for primary angle standards in metrology and achieve a high precision (within an uncertainty of 0.002″, k = 2) [15]-[17]. As both methods are based on elaborate measuring set-ups [18]-[21], [22] and [23] introduce two methods with much simpler realizations, one named prime factor division (PFD) enabling a shortening of the cross-calibration between two divided circles, and the other one named error frequency scanning self-calibration (EFSSC) suitable for sensors in harsh environments. However, those methods above have to position most reading heads accurately, which means they are restricted to performing with high precision sensors. Another type of methods do not need to position reading heads accurately, like TDR and redundant sampling self-calibration (RSSC), but TDR is sensitive to air bearing intrinsic torque [24], [25], and RSSC is invalid for some error harmonics [26], [27]. Consequently, those methods above are difficult to be widely applied, for that most elaborate measuring set-ups are hard to perform well in adverse environmental conditions which are commonly found in industrial rotating systems where there are oil, water, dust, vibration, and unstable ambient temperature; high precision sensors are hard to redundant cheaply; and high precision non-rolling element bearings are not used in all industrial rotary system.

In this paper, a coaxial sensors relative rotation self-calibration method named CSRR is presented. To make this method be more of interest for practical applications, the inductive time grating angular displacement sensors, which have superior performance in harsh working environments and cheaper than most sensors of the same precision [28]-[30], are chosen to be self-calibrated. In the same condition, besides general advantages of self-calibration method, this method can avoid elaborate measuring set-ups that exist in those ones like EDA. It is insensitive to bearing intrinsic torque and valid for more error harmonics than RSSC. In addition, it can perform self-calibration of sensors on their application axes by only a few slight modifications to the machine.

This work was supported by National Natural Science Foundation of China under Grant 51475063, Grant 51605062 and Grant 51675071. (Corresponding author: Donglin Peng.)

L. Gou is with the School of Instrumentation Science and Opto-electronics Engineering, Hefei University of Technology, Hefei 230009, China (e-mail: qq392803277@126.com).

D. L. Peng, X. H. Chen, L. Wu and Q. F. Tang are with Engineering Research Center of Mechanical Testing Technology and Equipment ,Ministry of Education, Chongqing University of Technology, Chongqing 400054, China (e-mail: pdl@cqut.edu.cn; cxh0458@cqut.edu.cn; wh0219@cqut.edu.cn; sealyl@126.com).

This article has been accepted for publication in a future issue of this journal, but has not been fully edited. Content may change prior to final publication. Citation information: DOI 10.1109/JSEN.2018.2879099, IEEE Sensors Journal

II. CSRR Self-Calibration Method

A. Time Grating Sensor

Time grating sensor mentioned to be self-calibrated is an inductive angular displacement sensor. It measures the angular displacement from the change in time lag between two pulse sequences, which are, respectively, excitation pulse sequence generated by excitation rotating magnetic field and induction pulse sequence generated by induction rotating magnetic field modulated by angular displacement, as shown in Fig. 1.

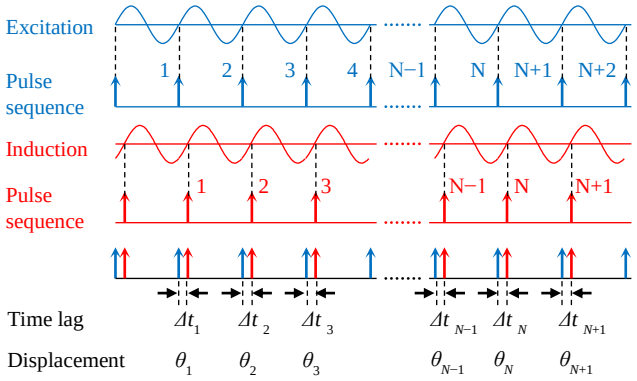

Fig. 1. Measurement principle of time grating sensor.

With the help of symmetrical structure, most electromagnetic noise of time grating sensor can be canceled. And since this sensor is also helped by evenly distributed pole-pairs, the main harmonic component frequencies of its system error are integral multiple of the number of pole-pairs. Take a 72 pole-pairs time grating sensor as an example, the main harmonic component frequencies of its system error are 72, 144, 216, 288, etc. Thus, if two time grating sensors are different in the number of pole-pairs, most main harmonic frequencies of their system errors are different. These features will be used later.

B. Basic Principle

The angular displacement synchronous measurements of two coaxial sensors can be modeled as

$$\begin{cases} f_a(\theta) = \theta + \varepsilon_a(\theta) \\ f_b(\theta - \Delta_{ab}) = \theta - \Delta_{ab} + \varepsilon_b(\theta - \Delta_{ab}), \end{cases} \tag{1}$$

where θ is true value of synchronous angular displacement, $\varepsilon_a(\theta)$ and $\varepsilon_b(\theta-\Delta_{ab})$ are errors of sensor A and sensor B respectively and Δ_{ab} is the angle between their initial scales. So the difference between the two measurements is written as

$$f_{ab}(\theta) = \Delta_{ab} + \varepsilon_a(\theta) - \varepsilon_b(\theta - \Delta_{ab}). \tag{2}$$

According to circular closure principle, $\varepsilon_a(\theta)$ and $\varepsilon_b(\theta-\Delta_{ab})$ are periodic functions and Dirichlet Conditions could be easily proved. Thus the Fourier transform of (2) can be written as

$$F_{ab}(\omega) = \Delta_{ab} + F_a(\omega) - e^{j\omega\Delta_{ab}} F_b(\omega), \tag{3}$$

where $F_a(\omega)$ and $F_b(\omega)$ are the Fourier transform of $\varepsilon_a(\theta)$ and $\varepsilon_b(\theta)$ respectively. Then the DC component of $f_{ab}(\theta)$ can be expressed as

$$F_{ab}(0) = \Delta_{ab} + F_a(0) - F_b(0). \tag{4}$$

Since $F_a(0)$ and $F_b(0)$ are constant in general, the DC component $F_{ab}(0)$ varies with Δ_{ab}, the relative rotation angle of the two coaxial sensors. Thus if Δ_{ab}, the angle between initial scales of the two sensors, changes from 0 to Δ, then Δ can be expressed as

$$\Delta = F_{ab}(0)\big|_{\Delta_{ab}=\Delta} - F_{ab}(0)\big|_{\Delta_{ab}=0}. \tag{5}$$

By replacing Δ_{ab} in (1) with Δ in (5), the error of sensor B can be expressed as

$$\varepsilon_b(\theta - \Delta) = f_b(\theta - \Delta) + F_{ab}(0)\big|_{\Delta_{ab}=\Delta} - F_{ab}(0)\big|_{\Delta_{ab}=0} - \theta. \tag{6}$$

When Δ varies from 0 to 2π, if θ is constant, the error of sensor B can be obtained. As the repeatability error of self-calibrated sensor should be very small, the true positions with the same measured value almost coincide. Thus the measured value of sensor A can be used as a benchmark to fix θ. For instance, if $f_a(\theta_a)$=0 is the benchmark, the true position θ is fixed to be constant θ_a when the measured value of sensor A is zero. Thus by replacing θ in (6) with θ_a, sensor B can be self-calibrated, as expressed in (7).

$$\varepsilon_b(\theta_a - \Delta) = f_b(\theta_a - \Delta) + F_{ab}(0)\big|_{\Delta_{ab}=\Delta} - F_{ab}(0)\big|_{\Delta_{ab}=0} - \theta_a, \tag{7}$$

where θ_a is a constant and has no effect on the angular displacement calibration. Obviously, the errors of both sensors can be self-calibrated in the same way.

C. Error Evaluation of CSRR

When high sampling frequency is adopted, random error mostly has little effect on (4). Thus this self-calibration method is mainly affected by the relative rotation error of two coaxial sensors and the uniformity of sampling.

When the coaxial sensors rotate relative, for instance sensor B rotates around the stationary sensor A and Δ_{ab} changes from 0 to Δ, if their gyration centers do not coincide, ε_b may be changed to $\varepsilon_b+\varepsilon_r$, where ε_r is the additional error caused by relative rotation. If the sampling uniformity is good enough, the effect of relative rotation error can be added directly to (4) and be expressed as

$$F_{ab}(0) = \Delta_{ab} + F_a(0) - F_b(0) - F_r(0), \tag{8}$$

where $F_r(\omega)$ is the Fourier transform of relative motion error ε_r, and $F_r(0)$ is the DC component of $F_r(\omega)$. Since the gyration centers of coaxial sensors will not change observably after the coaxial sensors are both built into the machine, the additional error caused by their non-coincidence will not change observably either. Thus the $F_r(0)$ can be assumed to be constant and has no effect on this self-calibration principle, just as the θ_a in (7).

If the sampling uniformity is poor, the effect of it also should be taken into consideration. Assuming the sampling position $\theta(n)$ can be expressed as

$$\theta(n) = n\theta_0 + \varepsilon_\theta(n), \tag{9}$$

where n changes from 1 to $2N$, θ_0 is average sampling interval, N times of θ_0 is π, and $\varepsilon_\theta(n)$ is the n^{th} difference between sampling position and average position. With the effect of $\varepsilon_\theta(n)$, $\varepsilon_a(\theta)$ and $\varepsilon_b(\theta)$ become frequency modulation signals and the Fourier transform of them are no longer $F_a(\omega)$ and $F_b(\omega)$. As the frequency modulation principle for each frequency component of the modulation signal is similar, it may be assumed that the modulation signal has single frequency, which means the Fourier transform of $\varepsilon_\theta(n)$ can be expressed as

$$F_\theta(\omega) = j\pi m_\Omega \left[\delta(\omega + \Omega) - \delta(\omega - \Omega)\right], \tag{10}$$

This article has been accepted for publication in a future issue of this journal, but has not been fully edited. Content may change prior to final publication. Citation information: DOI 10.1109/JSEN.2018.2879099, IEEE Sensors Journal

where Ω and m_Ω are frequency and amplitude of $\varepsilon_\theta(n)$ respectively. Thus affected by $\varepsilon_\theta(n)$, $F_a(\omega)$ can be represented as

$$F_{aJ}(\omega)=\pi\sum_{i=1}^{\infty}A_{\omega_i}\sum_{n=-\infty}^{\infty}J_n(\Omega m_\Omega)\left[e^{-j\varphi_{\omega i}}\delta(\omega+\omega_i+n\Omega)+e^{j\varphi_{\omega i}}\delta(\omega-\omega_i-n\Omega)\right]+A_0\delta(\omega), \tag{11}$$

where $A_{\omega i}$ and $\varphi_{\omega i}$ are amplitude and phase angle of $F_a(\omega_i)$ respectively and $J_n(\Omega m_\Omega)$ is the n^{th} order Bessel function of the first kind. The $J_n(x)$ could be expressed as

$$J_n(x)=\sum_{m=0}^{\infty}\frac{(-1)^m}{m!\Gamma(m+n+1)}\left(\frac{x}{2}\right)^{2m+n}. \tag{12}$$

Since $\varepsilon_\theta(n)$ can easily achieve a level smaller than milliradian, its amplitude, m_Ω, is usually very small. It is easy to ensure Ωm_Ω is far smaller than 1. When $\Omega m_\Omega \ll 1$, if the absolute value of integer n is larger than 1, the values of $J_n(\Omega m_\Omega)$ are much smaller than Ωm_Ω, and accordingly can be ignored. Consequently, when ω=0, the DC component of $F_{aJ}(\omega)$ can be expressed as

$$\begin{aligned}F_{aJ}(0)&=A_0-\pi\sum_{i=1}^{\infty}A_{\omega_i}\sum_{n=-1}^{1}J_n(\Omega m_\Omega)\left[e^{-j\varphi_{\omega i}}\delta(\omega_i+n\Omega)+e^{j\varphi_{\omega i}}\delta(-\omega_i-n\Omega)\right]\\&\approx A_0-\pi\sum_{i=1}^{\infty}A_{\omega_i}\left[\Omega m_\Omega\cos\varphi_{\omega i}\delta(\omega_i+\Omega)+\cos\varphi_{\omega i}\delta(\omega_i)-\Omega m_\Omega\cos\varphi_{\omega i}\delta(\omega_i-\Omega)\right].\end{aligned} \tag{13}$$

As Ω>0 and ω_i>0, $F_{aJ}(0)$ could be represented as

$$F_{aJ}(0)=A_0-\pi\Omega m_\Omega A_\Omega\cos\varphi_{A_\Omega}. \tag{14}$$

Similarly, affected by $\varepsilon_\theta(n)$, $F_b(\omega)$ and $F_r(\omega)$ can also be represented by $F_{bJ}(\omega)$ and $F_{rJ}(\omega)$ respectively. Then the DC component of them, $F_{bJ}(0)$ and $F_{rJ}(0)$, can be obtained. By replacing the DC components in (4) with $F_{aJ}(0)$, $F_{bJ}(0)$ and $F_{rJ}(0)$, the effect of $\varepsilon_\theta(n)$ on (5) can be expressed as

$$\begin{aligned}F_{J\Omega}(\Delta)&=F_{ab}(0)\big|_{\Delta_{ab}=\Delta}-F_{ab}(0)\big|_{\Delta_{ab}=0}-\Delta\\&=-\pi\Omega m_\Omega\left[A_\Omega\cos\varphi_{A_\Omega}-B_\Omega\cos\left(\varphi_{B_\Omega}-\frac{\Omega\Delta}{2\pi}\right)-R_\Omega\cos\left(\varphi_{R_\Omega}-\frac{\Omega\Delta}{2\pi}\right)\right],\end{aligned} \tag{15}$$

According to (5) and (7), $F_{J\Omega}(\Delta)$ is also the calibration error of CSRR method. Obviously, only the error harmonic of measurement system with frequency Ω will affect this self-calibration method, which means if an error harmonic with the same frequency as $\varepsilon_\theta(n)$ is small enough, there is little error after self-calibration.

In addition, under ideal conditions, if $R_{12}(\omega)$ is the Fourier transform of the cross-correlation between the error of measurement system and the change rate of sampling uniformity, the DC component of it can be written as

$$\begin{aligned}R_{12}(0)&=j\pi^2\Omega m_\Omega\left[A_\Omega\cos\varphi_{A_\Omega}-B_\Omega\cos\left(\varphi_{B_\Omega}-\frac{\Omega\Delta}{2\pi}\right)-R_\Omega\cos\left(\varphi_{R_\Omega}-\frac{\Omega\Delta}{2\pi}\right)\right]\\&=-j\pi F_{J\Omega}(\Delta).\end{aligned} \tag{16}$$

Thus if the modulation signal $\varepsilon_\theta(n)$ contains more than one significant frequency component, the calibration error of CSRR method can be expressed as

$$\begin{aligned}F_J(\Delta)&=\sum_{\Omega=1}^{N}F_{J\Omega}(\Delta)\\&=\frac{j}{\pi}\sum_{\Omega=1}^{N}R_{12}(0).\end{aligned} \tag{17}$$

Therefore, the CSRR method is insensitive to relative rotation error, and it is also insensitive to sampling uniformity in particular situation.

D. Effective Range of CSRR

Since some situations may make CSRR method susceptible to sampling uniformity, it is necessary to compare $F_{J\Omega}(\Delta)$ with the error of measurement system. If $F_{J\Omega}(\Delta)$ is much smaller than the other, this situation belongs to effective range of CSRR method.

If the sensors are calibrated on their application axis, the peak to peak value of $f_{ab}(\theta)-\Delta$ can be expressed as

$$\varepsilon_{pp}=2\sqrt{\alpha_\Omega^2+\beta_\Omega^2}. \tag{18}$$

where

$$\begin{cases}\alpha_\Omega=A_\Omega\cos\varphi_{A_\Omega}-B_\Omega\cos\left(\varphi_{B_\Omega}-\varphi_\Delta\right)-R_\Omega\cos\left(\varphi_{R_\Omega}-\varphi_\Delta\right)\\\beta_\Omega=A_\Omega\sin\varphi_{A_\Omega}-B_\Omega\sin\left(\varphi_{B_\Omega}-\varphi_\Delta\right)-R_\Omega\sin\left(\varphi_{R_\Omega}-\varphi_\Delta\right)\\\varphi_\Delta=\dfrac{\Omega}{2\pi}\Delta.\end{cases} \tag{19}$$

Then those situations which belong to effective range of CSRR method can be expressed by the proportion of $F_{J\Omega}$ to ε_{pp}, as

$$\left|\frac{F_{J\Omega}}{\varepsilon_{pp}}\right|=\left|\pi\Omega m_\Omega\frac{\alpha_\Omega}{2\sqrt{\alpha_\Omega^2+\beta_\Omega^2}}\right|\le 0.5\pi\Omega m_\Omega. \tag{20}$$

If the evaluation indicator for effective range of CSRR method is Y_Ω=0.5$\pi\Omega m_\Omega$, which is proportional to the product of the frequency and amplitude of the modulation function, the evaluation rules are shown in Fig. 2. The white area represents a calibration error of smaller than 1%, which means CSRR method is significantly effective in this area. And the black area represents a calibration error of larger than 100%, which means CSRR method is susceptible to sampling uniformity in this area.

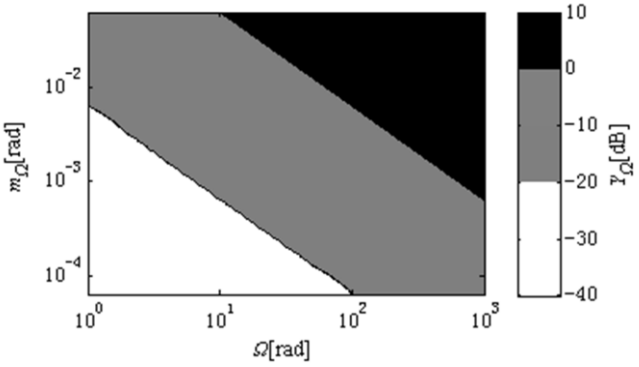

Fig. 2. The rules for evaluating the effective range of CSRR method.

III. Experimental Device and Procedure

A. Experimental Device

An experimental device is designed according to the

This article has been accepted for publication in a future issue of this journal, but has not been fully edited. Content may change prior to final publication. Citation information: DOI 10.1109/JSEN.2018.2879099, IEEE Sensors Journal

principle of CSRR, as shown in Fig. 3.

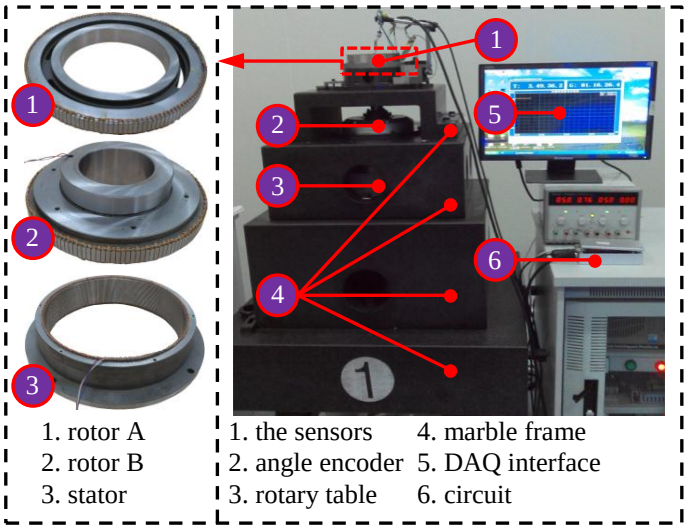

Fig. 3. Pictures of experimental device. (a) Structure of the sensors. (b) Overall view of experimental device.

The sensors to be self-calibrated consist of two coaxial rotors and a shared stator, as shown in Fig. 3 (a). Each rotor can provide its angular displacement independently. Rotor A can rotate about the shaft on rotor B to generate relative rotation angle of the two rotors and they can be also locked together. As shown in Fig. 3 (b), marble frame is a platform for installing the sensors, an angle encoder, a rotary table and a motor. The shaft connecting the rotor B and the shaft connecting the angle encoder are coaxial and they are driven by the rotary table. The angle encoder is used to examine the sensors. An industrial computer is equipped for the motor servo system and data acquisition (DAQ) system. The circuit for the sensors was integrated into a metal box in order to improve its stability, and it acquires position data of the sensors and angle encoder synchronously and transmits them to computer.

B. Experimental Procedure

According to the principle of CSRR, the two sensors should operate following the experimental procedure shown in Fig. 4. First, when rotor A has been locked to rotor B and they are rotating at a constant speed, sample the position data of two sensors synchronously and ensure that each of them cover angles from 0 to 2π. Then the sampling result is the first set of data. Second, unlock the two sensors and rotate rotor A alone at an angle of Δ. At last, lock the two sensors again and repeat as the first step, the second set of data can be obtained.

After that, according to the CSRR method, the error of sensor A (rotor A) at its angle Δ can be calculated by the two sets of data. Repeat the steps above with different relative rotation angles until enough errors are obtained to reconstruct the full error curve of sensor A. In addition, the full error curve of another sensor can be self-calibrated in the same way.

IV. Experimental Results

Both sensors used in first self-calibration experiment are 72 pole-pairs time grating sensors, their main characters are shown in table I.

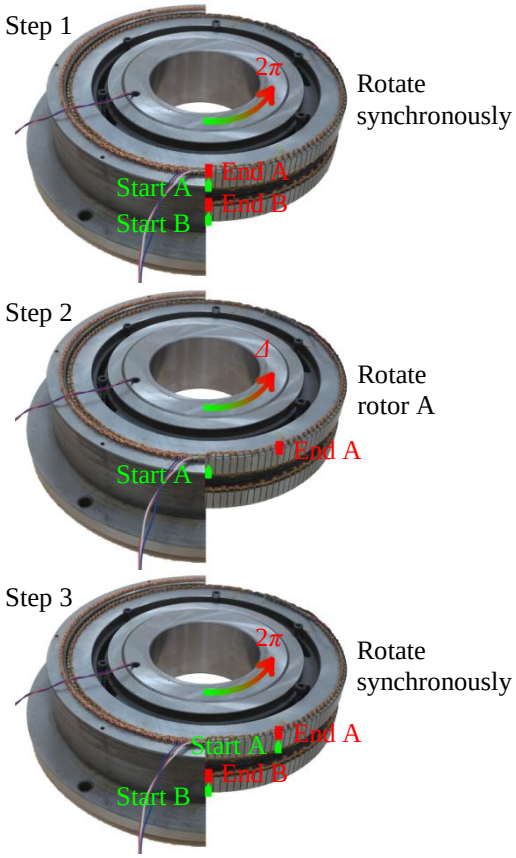

Fig. 4. Experimental procedure.

TABLE I
Main Characters of Time Grating Sensors in This Experiment

Characters	Value
System accuracy	±37″
Measurement frequency	400Hz
Counter frequency	80MHz
Theoretical resolution	0.09″

Before and after self-calibration, the errors of the sensor to be self-calibrated can be obtained by the angle encoder HEIDENHAIN RON886, of which the system accuracy is ±1″. The rotary table is driven by the motor servo system and rotates at a speed of 10 r/min. The error (stability) of speed is about 1% in closed loop condition and 10% in open loop condition. The rotational axis is supported by rolling bearing.

In closed loop condition, since the long-period error components of the self-calibrated sensor are not significant, partial angles (e.g. ones range from 0 to 10 degrees) are enough to show the main error features, as shown in Fig. 5. Compared with the RON886 encoder, before self-calibration, the error ranges from −17″ to 54″ and repeats twice significantly within 10 degrees, while after self-calibration, it has no longer obvious regulation and ranges from −0.4″ to 0.5″. In addition, still compared with the RON886 encoder, the long-period error component is reduced from ±3.1″ to ±0.9″ after self-calibration.

In the same condition, the EDA method and the TDR method are applied to self-calibrate the same time grating sensor. Table

This article has been accepted for publication in a future issue of this journal, but has not been fully edited. Content may change prior to final publication. Citation information: DOI 10.1109/JSEN.2018.2879099, IEEE Sensors Journal

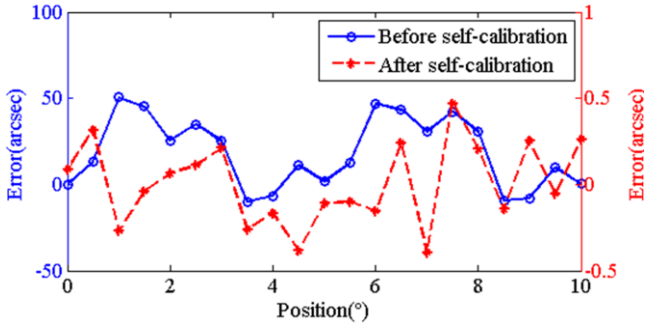

Fig. 5. Comparison of the errors of Δ in (0°-10°) before and after self-calibration.

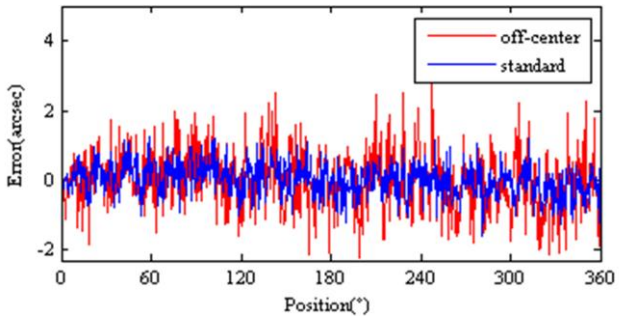

Fig. 6. Comparison of the errors of Δ in (0°-360°) by standard and off-center state.

II shows a comparison of the main 6 harmonic amplitudes of self-calibrated sensor error maps derived from TDR, EDA and CSRR methods. The maximum difference between Sensor-72 and CSRR is smaller than 1″, while that between Sensor-72 and TDR is larger than 4″. The results of EDA-5 are close to that of CSRR, but EDA-5 requires 1.5 times more sensors than CSRR because the EDA method is invalid for those error harmonics multiple of the number of its reading heads, which means at least 5 reading heads (sensors) are required to self-calibrate this 72 pole-pairs time grating sensor. Consequently, in this condition, compared with TDR, CSRR method performs better in calibration accuracy; and compared with EDA, CSRR method mostly requires fewer sensors to get the same calibration accuracy.

TABLE II
COMPARISON OF CALIBRATION ERROR MAPS FROM TDR, EDA AND CSRR METHODS

Frequency	Sensor-72	TDR	EDA-2	EDA-5	CSRR
72	23.87	20.12	N/A	24.61	23.81
216	14.03	9.81	N/A	13.17	13.98
144	5.27	4.31	N/A	4.76	5.23
1	2.34	4.82	2.04	1.87	1.96
2	1.68	1.97	N/A	1.32	1.45
432	0.96	0.66	N/A	0.93	0.92

Sensor-72: the main harmonic amplitudes of self-calibrated 72 pole-pairs time grating sensor error maps derived from angle encoder; TDR: TDR self-calibration method [24]; EDA-2: EDA self-calibration method with 2 reading heads; EDA-5: EDA self-calibration method with 5 reading heads [13]. The error map harmonic amplitudes are in arc-sec.

A. Calibration Accuracy Verification of Relative Rotation Error

According to the experimental procedure, relative rotation error may occur in step 2 due to the relative rotation caused by rotor A rotating about the shaft on rotor B. In order to lay stress on the effect of relative rotation error on calibration accuracy, an excentric sleeve is added to the shaft on rotor B, and rotor A rotate about it in step 2. If the standard state is that rotor A rotate about the shaft on rotor B and the off-center state is that rotor A rotating about the excentric sleeve, when the measured value of sensor B is zero, the error of sensor A is approximately ±37" in standard state and ±59" in off-center state. Then sensor A can be self-calibrated in standard state and off-center state. By comparing the two results, the effect of relative rotation error on calibration accuracy is shown in Fig. 6.

Though the peak-to-peak value of the off-center one is slightly larger than that of the other, the peak-to-peak value of the difference between two results is smaller than 2.2″, which is only 5% of the effect on accuracies of sensors caused by relative rotation error. Thus the relative rotation error has little effect on calibration accuracy.

B. Calibration Accuracy Verification of Poor Sampling Uniformity

According to (15), system errors of the two sensors have to be large enough to get a significant effect on the calibration accuracy in the case of poor sampling uniformity. Thus another two sets of sensors are chosen for self-calibration. First set is two 84 pole-pairs time grating sensors with system accuracy of approximately ±680", and second set is two 90 pole-pairs ones with system accuracy of approximately ±250". The other characters of the sensors are the same to those of 72 pole-pairs one. And the rotary table rotates in an open loop condition at a speed of 10 r/min to provide worse sampling uniformity $\varepsilon_\theta(n)$. After self-calibration, the results are shown in Fig. 7.

Before and after the self-calibration, for the self-calibrated sensor of first set, its error is reduced from larger than ±680" to smaller than ±2" and it has no significant regulation, whereas for the second set, it is reduced from approximately ±280" to about ±10" and it repeats 2.5 times within 10 degrees. Obviously, poor sampling uniformity does not always affect the accuracy of self-calibration.

To quantitatively verify when and how sampling uniformity affect the accuracy of self-calibration, according to (17), the Fourier transform of the cross-correlation $|R_{12}(0)|$ needs to be calculated. Since the error of encoder is far smaller than the peak-to-peak value of sampling uniformity, the difference $\varepsilon_\theta(n)$ between sampling position and average position can be replaced by the change in the synchronous measurement increment of the encoder. And since it is easy to make the relative rotation error much smaller than errors of this two set of sensors (e.g. when Δ=2 °in first set and Δ=4 °in second set, the absolute values of the errors of Δ before and after self-calibrations may approach the maximum simultaneously), for each set, the parameter α_Ω can be approximated by the coefficients of the Fourier series of the two sensors. Thus $|R_{12}(0)|$ can be approximated with the help of synchronous encoder, as shown in table III.

This article has been accepted for publication in a future issue of this journal, but has not been fully edited. Content may change prior to final publication. Citation information: DOI 10.1109/JSEN.2018.2879099, IEEE Sensors Journal

TABLE III
EFFECT OF POOR SAMPLING UNIFORMITY

Frequency	Amplitude of $\varepsilon_\theta(n)$	First set (Δ=2 °)			Second set (Δ=4 °)		
$\Omega/2\pi$ (Hz)	m_Ω (″)	α_Ω (″)	$\lvert R_{12}(0)\rvert$ (″)	$\lvert F_{J\Omega}\rvert$ (″)	α_Ω (″)	$\lvert R_{12}(0)\rvert$ (″)	$\lvert F_{J\Omega}\rvert$ (″)
1	59.89	7.524	0.1355	< 0.1	15.37	0.2769	< 0.1
2	19.00	20.03	0.2288	< 0.1	1.457	0.0167	< 0.1
45	17.06	0.1087	0.0251	< 0.1	0.7678	0.1773	< 0.1
4	15.39	2.625	0.0486	< 0.1	1.494	0.0276	< 0.1
810	11.71	0.0092	0.0261	< 0.1	0.2384	0.68	< 0.2
6	10.60	0.6328	0.0121	< 0.1	0.223	0.0043	< 0.1
5	9.265	0.4387	0.0061	< 0.1	1.167	0.0225	< 0.1
7	8.478	0.2821	0.0050	< 0.1	0.4774	0.0085	< 0.1
90	7.734	2.885	0.6036	0.58	121.0	25.32	7.66

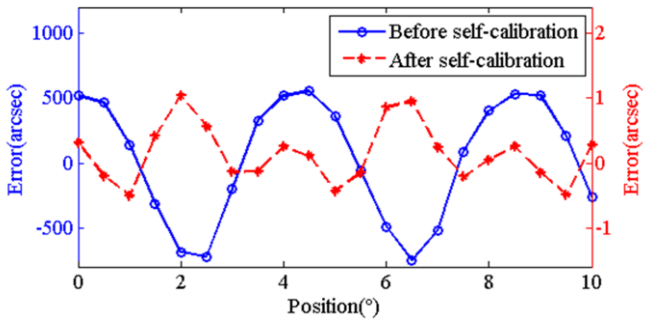

(a)

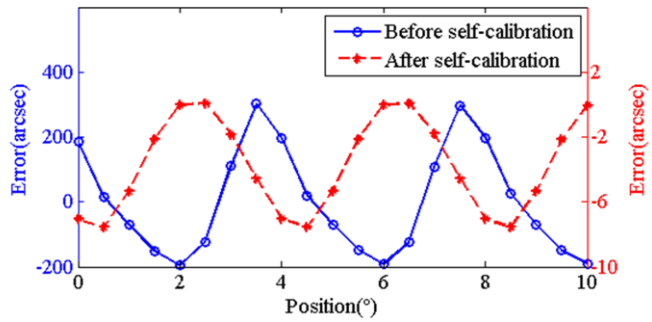

(b)

Fig. 7. Comparison of self-calibration accuracies of two sets of sensors in poor sampling uniformity. (a) First set sensors with ±680" system accuracy. (b) Second set sensors with ±250" system accuracy.

Table III is listed in descending order according to the Amplitude of $\varepsilon_\theta(n)$ within 1000 harmonics, and the error of Δ for each set obtained by encoder is given following each $|R_{12}(0)|$. Obviously, at the main frequency of $\varepsilon_\theta(n)$ shown in table III, the residual errors $|F_{J\Omega}(\Delta)|$ of the first set are all small, and its maximum value is still smaller than the system accuracy of the encode. Though those of the second set are also small except the one at 90Hz, the exception frequency is just one of the main error frequencies of $\varepsilon_\theta(n)$. And that exception frequency is equal to the number of pole-pairs of sensors in second set, which means it is also one of the main error frequencies of self-calibrated sensor. Thus if all of the main error frequencies of $\varepsilon_\theta(n)$ is not the integral multiple of the number of pole-pairs of self-calibrated sensor, as the conditions of first set, after self-calibration, the residual error can be smaller than 0.3%. Otherwise, as the conditions of second set, after self-calibration, the residual error can be larger even though the system error of its self-calibrated sensor is smaller than that of the other one. And the main error frequencies of $\varepsilon_\theta(n)$ will not change in a same machine. Thus according to the error sources of the time grating sensor described in Section 2, two sets of time grating sensors with different numbers of pole-pairs are enough to ensure that condition described above, which means it is easy to ensure the CSRR method insensitive to sampling uniformity. In addition, according to (15) and (17), when any of the main error frequencies of $\varepsilon_\theta(n)$ is the integral multiple of the number of pole-pairs of self-calibrated sensor, the higher that frequency is, the larger the residual error is.

As shown at 90Hz in table III, since the $|R_{12}(0)|$ and $|F_{J\Omega}(\Delta)|$ of the second set are close to the regulation of (16), $|F_{J\Omega}(\Delta)|$, the main effect of $\varepsilon_\theta(n)$ on the accuracy of self-calibration, can be approximated by $|R_{12}(0)|/\Omega$, which may make spectrum analysis of $|F_{J\Omega}(\Delta)|$ easier.

In the same conditions (rotational axis is supported by rolling bearing), the EDA method and TDR method are applied to self-calibrate 84 pole-pairs time grating sensor of first set. Table IV shows a comparison of the main harmonic amplitudes of self-calibrated sensor error maps derived from TDR, EDA and CSRR methods. The maximum difference between Sensor-84 and CSRR is smaller than 1″, while that between Sensor-84 and TDR is larger than 56″ and that between Sensor-84 and EDA-5 is larger than 35″. According to [24], TDR method achieves very high calibration accuracy (±0.2") on the rotational axis supported by air bearing. But combining results of TDR in table II and table IV, obviously, TDR method cannot achieve that high calibration accuracy when the

TABLE IV
COMPARISON OF CALIBRATION ERROR MAPS FROM TDR, EDA AND CSRR METHODS

Frequency	Sensor-84	TDR	EDA-5	CSRR
84	668.95	612.17	633.07	668.68
168	104.19	87.31	93.44	104.08
252	35.56	21.83	30.32	35.52
2	20.03	24.52	19.98	19.64
1	7.52	19.09	7.49	7.06
336	5.82	3.88	4.62	5.79

Sensor-84: the main harmonic amplitudes of self-calibrated 84 pole-pairs time grating sensor error maps derived from angle encoder; TDR: TDR self-calibration method at 10 rpm; EDA-5: EDA self-calibration method with 5 reading heads. The error map harmonic amplitudes are in arc-sec.

This article has been accepted for publication in a future issue of this journal, but has not been fully edited. Content may change prior to final publication. Citation information: DOI 10.1109/JSEN.2018.2879099, IEEE Sensors Journal

rotational axis is supported by rolling bearing. According to the principle of EDA method [13], its calibration accuracy will not be affected by the sampling uniformity. However, when the system error of self-calibrated sensor is as large as that shown in Fig. 7(a), the EDA method cannot perform well in calibration accuracy. Consequently, compared with TDR, CSRR method performs much better on the axis supported by rolling bearing; and compared with EDA, , in this condition, CSRR method can achieve higher calibration accuracy.

C. Effective Range Verification

In table V, according to (19), the main evaluation indicators $|Y_{\Omega}|$ within 1000 harmonics are listed in descending order, and amplitude of the error of self-calibrated sensor for each set is given following it. Obviously, most $|Y_{\Omega}|$ listed in table V are larger than 1% and belong to the gray area in Fig. 2, where the CSRR method is not reliable or effective. If the amplitudes of error harmonics of self-calibrated sensor at these frequencies are small, like those in first set(third column of table V), then the CSRR method is still significantly effective, as shown in Fig. 7(a). Otherwise, if some amplitudes of error harmonics of self-calibrated sensor at these frequencies are much larger than others, like that at 90Hz in second set(fourth column of table V), the residual error of self-calibrated sensor($|Y_{\Omega}|A_{\Omega}$=4.73″) may be too large to trust this method, as shown in Fig. 7(b).

TABLE V
MAIN FREQUENCY OF EVALUATION INDICATORS $|Y_{\Omega}|$

Frequency $\Omega/2\pi$ (Hz)	Evaluation $\lvert Y_{\Omega}\rvert$	First set A_{Ω} (″)	Second set A_{Ω} (″)
810	0.4540	0.0092	0.2384
809	0.0768	0.0027	0.0176
45	0.0367	0.0787	0.7678
90	0.0333	1.985	142.1
540	0.0303	0.0154	1.453
630	0.0232	0.0089	0.5015

Since the analysis above is consistent with the experimental results of Fig. 7 and table III, it is reliable to evaluate the effective range of the CSRR method with $|Y_{\Omega}|$. Though $|R_{12}(0)|$ can also be used to evaluate the effective range, the use of it is more complicated than that of $|Y_{\Omega}|$ because it requires more measurements and calculations. Thus evaluation indicators $|Y_{\Omega}|$ may make it easier to analyze the effective range of CSRR method.

V. CONCLUSION

A new self-calibration method for angular displacement sensor, named *coaxial sensors relative rotation* (CSRR) method, has been described in theory and tested experimentally. For this method, if the two coaxial sensors always start their full period sampling from a particular measured value of one of them, the error of relative rotation angle (the angular displacement of the other sensor) can be self-calibrated by the sampling data before and after the two sensors rotate relatively. With enough relative rotation angles (range from 0 to 360°) been self-calibrated, the error curve of the other sensor can be obtained. In addition, each of the two coaxial sensors can be self-calibrated in this way.

The experimental results demonstrated calibration accuracy of ±1.5″ compared with a given high precision encoder, when the system error of sensor is about ±37″ and the sampling uniformity is good. By the relative rotation error experiment, it is verified that the relative rotation error has little effect on calibration accuracy. And by the contrast experiments, they are verified that: the EDA method mostly requires more sensors than CSRR method to get the same calibration accuracy; the TDR method cannot perform well on the axis supported by rolling bearing, but CSRR method can; and two sets of time grating sensors with different numbers of pole-pairs are enough to ensure the CSRR method insensitive to sampling uniformity.

In addition, an evaluation indicator $|Y_{\Omega}|$ is proposed, which has verified to be reliable in evaluating the effective range of the CSRR method. Thus with the help of $|Y_{\Omega}|$, it is easy to know whether this method is suitable for sensors to be self-calibrated.

REFERENCES

[1] W. Gao *et al.*, "Measurement technologies for precision positioning," *CIRP Ann.-Manuf. Technol.*, vol. 64, no. 2, pp. 773–796, Jun. 2015.

[2] A. J. Fleming, "A review of nanometer resolution position sensors: Operation and performance," *Sens. Actuators A, Phys.*, vol. 190, pp. 106–126, Feb. 2013.

[3] Y. Jia, S.L. Li, Y.Y. Qin, and R.C. Cheng, "Error analysis and compensation of MEMS rotation modulation inertial navigation system," *IEEE Sensors J.*, vol. 18, no. 5, pp. 2023–2030, Mar. 2018.Z. Wu, and Y.L. Li, "High-accuracy automatic calibration of resolver signals via two-step gradient estimators," *IEEE Sensors J.*, vol. 18, no. 7, pp. 2883–2891, Apr. 2018.

[4] R. Markovic, A. Krajnc, D. Matko, "Calibration of a solid-state magnetic compass using angular-rate information from low-cost sensors," *IET Sci. Meas. Technol.*, vol. 5, no. 2, pp. 54–58, Mar. 2011.

[5] R. Hoseinnezhad, A. Bab-Hadiashar, and P. Harding, "Calibration of resolver sensors in electromechanical braking systems: a modified recursive weighted least-squares approach," *IEEE Trans. Ind. Electron.*, vol. 54, no. 2, pp. 1052–1060, Apr. 2007.

[6] E.E. Aktakka, J.K. Woo, D. Egert, R.J.M. Gordenker, and K. Najafi, "A microactuation and sensing platform with active lockdown for in situ calibration of scale factor drifts in dual-axis gyroscopes," *IEEE/ASME Trans. Mechatronics*, vol. 20, no. 2, pp. 934–943, Apr. 2015.

[7] V. Giniotis, and M. Rybokas, "Traceability enhancement in angle measurements," *Measurement*, vol. 42, pp. 1516–1521, Aug. 2009.

[8] A. Bünte, and S. Beineke, "High-performance speed measurement by suppression of systematic resolver and encoder errors," *IEEE Trans. Ind. Electron.*, vol. 51, no. 1, pp. 49–53, Feb. 2004.

[9] P.Y. Gao, K. Li, T.X. Song, and Z.J. Liu, "An accelerometers-size-effect self-calibration method for triaxis rotational inertial navigation system," *IEEE Trans. Ind. Electron.*, vol. 65, no. 2, pp. 1655–1664, Feb. 2018.

[10] P.Y. Gao, K. Li, L. Wang, and J.X. Gao, "A self-calibration method for non-orthogonal angles of gimbals in tri-axis rotational inertial navigation system," *IEEE Sensors J.*, vol. 16, no. 24, pp. 8998–9005, Dec. 2016.

[11] C.H. Ren, Q.Q Liu, and T.D. Fu, "A novel self-calibration method for MIMU," *IEEE Sensors J.*, vol. 15, no. 10, pp. 5416–5422, Oct. 2015.

[12] J. Faber, "Self-calibration and noise reduction of resolver sensor in servo drive application," in *Proc. IEEE ELEKTRO*, May 2012, pp. 174–178.V.D. Aksenenko, and S.I. Matveyev, "Digital angle sensor self-calibration: two approaches to accuracy increasing," in *Proc. IEEE IMTC*, May 2005, pp. 543–547.

[13] T. Watanabe, H. Fujimoto, K. Nakayama, T. Masuda, and M. Kajitani, "Automatic high-precision calibration system for angle encoder," in *Proc. LMAC*, Munich, Germany, June 2001, pp. 267-274.

[14] R. Probst, R. Wittekopf, M. Krause, H. Dangschat, and A. Ernst, "The new PTB angle comparator," *Meas. Sci. Technol*., vol. 9, pp. 1059–1066, Mar. 1998.

[15] W. Kokuyama, T. Watanabe, H. Nozato, and A. Ota, "Angular velocity calibration system with a self-calibratable rotary encoder," *Measurement*, vol. 82, pp. 246–253, Jan. 2016.

This article has been accepted for publication in a future issue of this journal, but has not been fully edited. Content may change prior to final publication. Citation information: DOI 10.1109/JSEN.2018.2879099, IEEE Sensors Journal

[16] R.D. Geckeler, A. Link, M. Krause, and C. Elster, "Capabilities and limitations of the self-calibration of angle encoders," *Meas. Sci. Technol*., vol. 25 (055003), pp. 1–10, May. 2014.
[17] A. Just, M. Krausea, R. Probst, H. Bosse, H. Haunerdinger, Ch. Spaeth, G. Metz, and W. Israel, "Comparison of angle standards with the aid of a high-resolution angle encoder," *Precision Engineering*, vol. 33, pp. 530–533, Feb. 2009.
[18] T. Watanabe, M. Kon, N. Nabeshima, and K. Taniguchi, "An angle encoder for super-high resolution and super-high accuracy using SelfA," *Meas. Sci. Technol*., vol. 25, no. 6, pp. 65–71, Apr. 2014.
[19] T. Watanabe, H. Fujimoto, and T. Masuda, "Self-calibratable rotary encoder," in *Proc. JPCS*, Sep 2005, pp. 240-245.
[20] T. Yandayan, R. D. Geckeler, A. Just, M. Krause, S. A. Akgoz, M. Aksulu, B. Grubert, and T. Watanabe, "Investigations of interpolation errors of angle encoders for high precision angle metrology," *Meas. Sci. Technol*., vol. 29 (064007), pp. 1–10, May. 2018.
[21] R. D. Geckeler, and A. Just, "A shearing-based method for the simultaneous calibration of angle measuring devices," *Meas. Sci. Technol*., vol. 25 (105009), pp. 1–10, Oct. 2014.
[22] R. Probst, "Self-calibration of divided circles on the basis of a prime factor algorithm," *Meas. Sci. Technol*., vol. 19 (055003), pp. 1–11, Jan. 2008.
[23] J. Lu, X.H. Chen, Q.F. Tang, and L.B. Suo, "Fixed distance transform and error frequency scanning self-calibration method for time grating sensor," *Chinese Journal of Scientific Instrument*, vol. 37, no. 1, pp. 32–39, May. 2016.
[24] X.D. Lu, D.L. Trumper, "Self-calibration of on-axis rotary encoders," *CIRP Annals*, vol. 56, no. 1, pp. 499–504, Jun. 2009.
[25] X.D. Lu, R. Graetz, D. Amin-Shahidi, K. Smeds, "On-axis self-calibration of angle encoders," *CIRP Annals-Manufacturing Technology*, vol. 59, no. 1, pp. 529–534, May. 2007.
[26] L. Gou, X.H. Chen, D.L. Peng, L. Wu, and Q.F. Tang, "A redundant sampling self-calibration method based on single reading head of time grating sensor," *Chinese Journal of Scientific Instrument*, vol. 39, no. 3, pp. 124–131, Mar. 2018.
[27] X.H. Chen, L. Gou, Y.L. Guan, L.B. Suo, and Q. Zhou, "A self-calibration method of angular displacement sensor based on single reading head," *Chinese Journal of Sensors and Actuators*, vol. 27, no. 8, pp. 1049–1053, Aug. 2014.
[28] K. Peng, X. Liu, Z. Chen, Z. Yu, and H. Pu, "Sensing mechanism and error analysis of a capacitive long-range displacement nanometer sensor based on time grating," *IEEE Sensors J.*, vol. 17, no. 3, pp. 1596–1607, Mar. 2017.
[29] X. Liu, K. Peng, Z. Chen, H. Pu, and Z. Yu, "A new capacitive displacement sensor with nanometer accuracy and long range," *IEEE Sensors J.*, vol. 16, no. 8, pp. 2306–2316, Apr. 2016.
[30] Q.F. Tang, D.L. Peng, W. Liang, and X.H. Chen, "An inductive angular displacement sensor based on planar coil and contrate rotor," *IEEE Sensors J.*, vol. 16, no. 7, pp. 3947–3954, Jul. 2015.

Li Gou, received the M.Eng. degree in instrument engineering from the Chongqing University of Technology, Chongqing, China, in 2016. He is currently pursuing the Ph.D. degree with the School of Instrumentation Science and Optoelectronics Engineering, Hefei University of Technology, with a focus on precision measurement technologies and instruments of displacement.

Donglin Peng received the M.Eng. and Ph.D. (Eng.) degrees from Chongqing University, in 1988 and 1992, respectively. He was with the State Key Laboratory of Mechanical Transmission, Chongqing University, from 1982 to 2000. Since 2000, he has been with the Chongqing University of Technology. His research interests include precision measurement technologies and instruments.

Xihou Chen received the M.Eng. and Ph.D. (Eng.) degrees from Chongqing University, in 2004 and 2007, respectively. Since 2007, he has been a Professor with the Chongqing University of Technology. He mainly focuses on the research of displacement sensors and technologies of precision mechanical measurement.

Liang Wu received the Ph.D. (Eng.) degree from Chongqing University in 2017. He is currently an Associate Research Fellow with the Engineering Research Center of Mechanical Testing Technology and Equipment (Ministry of Education), Chongqing University of Technology. His research interests are modeling and simulation of sensors for displacement measurement.

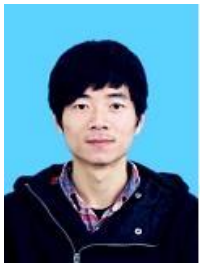

Qifu Tang received the Ph.D. (Eng.) degree from Chongqing University in 2015. He is currently an Associate Research Fellow with the Engineering Research Center of Mechanical Testing Technology and Equipment (Ministry of Education), Chongqing University of Technology. He mainly focuses on precision measurement technologies and instruments of displacement.